On the Stability of Bipedal Walking

Pieter van Zutven, Dragan Kostić, and Henk Nijmeijer

Eindhoven University of Technology, Faculty of Mechanical Engineering,
Dynamics and Control group, 5600 MB Eindhoven, The Netherlands,
p.w.m.v.zutven@tue.nl

Abstract. Stability of bipedal locomotion is analyzed using a model of a planar biped written in the framework of systems with unilateral constraints. Based on this model, two different stable walking gaits are derived: one which fulfills the widely used criterion of the Zero Moment Point (ZMP) and another one violating this criterion. Both gaits are determined using systematic model-based designs. The model and the two gaits are used in simulations to illustrate conservatisms of two commonly used methods for stability analysis of bipedal walking: the ZMP criterion and Poincaré return map method. We show that none of these two methods can give us a general qualification of bipedal walking stability.

Keywords: humanoid robotics, bipedal locomotion, stability analysis, zero moment point, Poincaré return map

1 Introduction

Stability analysis of bipedal walking is dificult, since dynamics of the bipedal robots are highly non-linear, under actuated, subject to impacts, variable external forces, and discrete changes between different modes. The common strategies, such as analysis of the eigenvalues, gain and phase margins or Lyapunov stability theory, can be applied to particular modes, such as a single or double stance, but are usually incapable to characterize stability of all modes in total. So far, stability of bipedal walking is analyzed by specific techniques, such as Zero Moment Point (ZMP) [1], Poincaré return maps [2], [3], [4], Foot Rotation Indicator [5], the theory of capture points [6], and the the foot placement estimator [7].

In this paper we analyze stability of bipedal locomotion using a model of a planar biped. The Lagrange-Euler equations of motion of the bipedal robot are represented in the framework of systems with unilateral constraints [8], by implementing set-valued force laws for normal contact and tangential Coulomb friction. Taking these effects into account is crucial for accurate dynamical modeling of the biped. The derived model is used in systematic design of two different stable walking gaits: one which fulfills the widely used ZMP-criterion and another one violating this criterion. The same model is later on used in simulations to illustrate conservatisms of two commonly used methods for stability analysis of bipedal walking: the ZMP criterion and Poincaré return map method.

There are two major contributions of this paper. First, we develop a model of a bipedal robot using the framework of systems with unilateral constraints.

The second contribution is a systematic model-based design of a limit-cycle walking (LCW) gait [3]. Finally, we illustrate, by means of simulations, serious conservatism of two of the most common stability criteria for bipedal walking, namely the methods of ZMP and the Poincaré mapping. Numerical illustrations of their conservatism are seldom in the literature. The numerical results given in this paper confirm that neither criterion can be used to establish stability of an arbitrary walking gait, which motivates further research towards more general qualification of stability of bipedal walking.

The paper is organized as follows. In Sect. 2, a model of a planar biped is described. In Sect. 3, a ZMP based and a LCW gait are derived. Stability of these gaits in analyzed in Sect. 4. Conclusions are given in Sect. 5.

2 Model of a Planar Biped

A model of a planar biped is introduced in this section. This model is used for design of walking gaits and stability analysis in Sects. 3 and 4, respectively.

2.1 Unconstrained Dynamics

We model dynamics of a planar bipedal robot with hips, knees and feet. A kinematics representation of this robot is shown in Fig. 1, with the coordinate frames assigned according to the Denavit-Hartenberg convention [9]. The robot consists of two upper legs, two lower legs and two feet. Consequently, six actuated degrees of freedom (dof's) are present. To facilitate derivation of the Lagrange-Euler equations of motion, a virtual robotic arm is attached to the hip. This arm adds two extra dof's that describe Cartesian motions of the robot relative to the world frame $[x_0, z_0]^T$. The equations of the unconstrained robot dynamics, i.e. the robot not being in contact with the ground, are derived using the Lagrange-Euler method [9] and presented here in standard form [8], [10]:

$$\boldsymbol{M}(\boldsymbol{q})\,\dot{\boldsymbol{u}} - \boldsymbol{h}(\boldsymbol{q}, \boldsymbol{u}) = \boldsymbol{\tau} \ , \tag{1}$$

where $\boldsymbol{q} \in \mathbb{R}^n$ is a minimal set of n generalized coordinates, $\boldsymbol{u} = \dot{\boldsymbol{q}}$, $\boldsymbol{M} \in \mathbb{R}^{n \times n}$ is the symmetric and positive definite inertia matrix, $\boldsymbol{h} \in \mathbb{R}^n$ is the vector containing all differentiable forces, such as gravitational forces and gyroscopic terms and $\boldsymbol{\tau} \in \mathbb{R}^n$ are the controller torques.

2.2 Contact Dynamics

Both feet of the biped can make contact with the ground with two contact points, located at the toe and heel. The contact points need to satisfy Signorini's set-valued force law, which states that the contact points cannot penetrate the ground. This results in a complementarity condition between the contact distance g_{Ni} and normal contact force λ_{Ni} at contact point $i \in \mathcal{I}_N$, where $\mathcal{I}_N$ is the set of n_N active contact points:

$$g_{Ni} \geq 0, \quad \lambda_{Ni} \geq 0, \quad g_{Ni}\lambda_{Ni} = 0 \ . \tag{2}$$

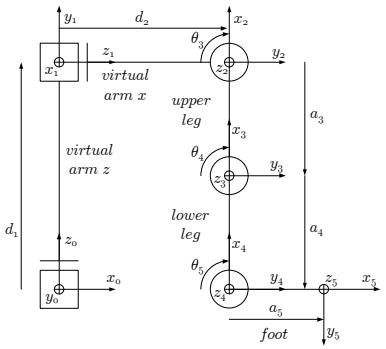

Fig. 1. Kinematic scheme of a planar bipedal robot with 6 actuated dofs

When the robot makes contact with the ground, an impact occurs. Newton's impact law is used to model these impacts. This law relates the pre- and post-impact velocity of contact point $i \in \mathcal{I}_N$ with a restitution coefficient e_{Ni}:

$$\gamma_{Ni}^{+} = e_{Ni}\gamma_{Ni}^{-} \ , \tag{3}$$

where $\gamma_{Ni} = \frac{d}{dt} g_{Ni}$. When a robot foot is in contact with the ground, it is subject to the ground friction. This is modeled using the Coulomb's friction law: at contact point $i \in \mathcal{I}_N$, the friction coefficient μ_i relates the friction force λ_{Ti} with the normal contact force λ_{Ni} and the tangential contact velocity γ_{Ti}:

$$\lambda_{Ti} \in -\mu_i \text{Sign}\left(\gamma_{Ti}\right) \lambda_{Ni}, \quad \text{Sign}\left(x\right) \in \begin{cases} \{-1\} & x < 0 \\ [-1,1] & x = 0 \\ \{1\} & x > 0 \end{cases} . \tag{4}$$

By combining the unconstrained equations of motion (1), Signorini's set valued contact law (2), Newton's impact law (3), and Coulomb's set valued friction law (4), we retrieve a new model of the dynamics of the planar bipedal robot with ground contact and tangential friction:

$$\begin{aligned} &\text{Constrained dynamics: } \boldsymbol{M}\dot{\boldsymbol{u}} - \boldsymbol{h} = \boldsymbol{\tau} + \boldsymbol{W}_N \boldsymbol{\lambda}_N + \boldsymbol{W}_T \boldsymbol{\lambda}_T \ , \\ &\text{Signorini's set valued contact law: } \boldsymbol{\gamma}_N \geq \boldsymbol{0}, \quad \boldsymbol{\lambda}_N \geq \boldsymbol{0}, \quad \boldsymbol{\gamma}_N^T \boldsymbol{\lambda}_N = 0 \ , \\ &\text{Coulomb's set valued friction law: } \boldsymbol{\lambda}_T \in -\boldsymbol{\mu}\text{diag}\left\{\text{Sign}\left(\boldsymbol{\gamma}_T\right)\right\} \boldsymbol{\lambda}_N \ , \\ &\text{Impact law: } \boldsymbol{\gamma}_N^{+} = \boldsymbol{e}_N \boldsymbol{\gamma}_N^{-} \ , \boldsymbol{\gamma}_T^{+} = \boldsymbol{e}_T \boldsymbol{\gamma}_T^{-} \ , \\ &\text{Generalized force directions: } \boldsymbol{W}_N = \left(\frac{\partial \boldsymbol{\gamma}_N}{\partial \boldsymbol{u}}\right)^T , \ \boldsymbol{W}_T = \left(\frac{\partial \boldsymbol{\gamma}_T}{\partial \boldsymbol{u}}\right)^T \ , \end{aligned} \tag{5}$$

where $\boldsymbol{\lambda}_N = \text{col}\left\{\lambda_{Ni}\right\} \in \mathbb{R}^{n_N}$, $\boldsymbol{\lambda}_T = \text{col}\left\{\lambda_{Ti}\right\} \in \mathbb{R}^{n_N}$, $\boldsymbol{\gamma}_N = \text{col}\left\{\gamma_{Ni}\right\} \in \mathbb{R}^{n_N}$, $\boldsymbol{\gamma}_T = \text{col}\left\{\gamma_{Ti}\right\} \in \mathbb{R}^{n_N}$, $\boldsymbol{\mu} = \text{diag}\left\{\mu_i\right\} \in \mathbb{R}^{n_N \times n_N}$, $\boldsymbol{e}_N = \text{diag}\left\{e_{Ni}\right\} \in \mathbb{R}^{n_N \times n_N}$ and $\boldsymbol{e}_T = \text{diag}\left\{e_{Ti}\right\} \in \mathbb{R}^{n_N \times n_N}$. Here, the contact equation is derived on the velocity level, in order to facilitate numerical integration. Notice that the contact equations are only valid for active contacts, i.e. $i \in \mathcal{I}_N$.

2.3 Numerical Integration

For numerical integration of the dynamical model (5), the time-stepping method of Moreau [11], [8], [10] can be used. This method use a time-discretization of generalized positions $\boldsymbol{q}$ and velocities $\boldsymbol{u}$. Forces acting on a system are taken into account in an integral way over every time step. This means that the time-stepping method does not make a distinction between impulsive and finite forces. The equations of motion are rewritten into measure differential equations [8], [10], which are not on the level of forces, but on the level of momenta. In this way only increments in position and velocity are computed. The acceleration is not used, as it might become infinite due to the impacts. The time-stepping method of Moreau is basically a midpoint differential algebraic equation-integrator. If events occur due to impact or release during a time step, it is not necessary to switch to another mode in the system model, because all forces are taken into account through their momenta in an integral. For the sake of numerical integration, the full set of equations of motion (5) needs to be written in equations rather than complementarity conditions. Using convex analysis and taking into account the notion of proximal point [8], [10], we can write the contact conditions as (implicit) equations. Furthermore, the equations of motion should be written as measure differential equations as stated before:

$$\begin{aligned} \boldsymbol{M}d\boldsymbol{u} - \boldsymbol{h}dt &= \boldsymbol{W}_N d\boldsymbol{\Lambda}_N + \boldsymbol{W}_T d\boldsymbol{\Lambda}_T \ , \\ d\boldsymbol{\Lambda}_N &= \mathrm{prox}_{C_N}\left(d\boldsymbol{\Lambda}_N - r\boldsymbol{\xi}_N\right) \ , \\ d\boldsymbol{\Lambda}_T &= \mathrm{prox}_{C_T}\left(d\boldsymbol{\Lambda}_T - r\boldsymbol{\xi}_T\right) \ , \end{aligned} \tag{6}$$

with

$$\begin{gathered} C_N = \mathbb{R}^+,\ C_T = \{d\boldsymbol{\Lambda}_T \mid -\boldsymbol{\mu}_T d\boldsymbol{\Lambda}_N \leq d\boldsymbol{\Lambda}_T \leq \boldsymbol{\mu}_T d\boldsymbol{\Lambda}_N\} \ , \\ \boldsymbol{\xi}_N = \boldsymbol{\gamma}_N^+ + \boldsymbol{e}_N\boldsymbol{\gamma}_N^-, \quad \boldsymbol{\xi}_T = \boldsymbol{\gamma}_T^+ + \boldsymbol{e}_T\boldsymbol{\gamma}_T^- \ , \\ \mathrm{prox}_C\left(\boldsymbol{z}\right) = \underset{\boldsymbol{x}\in C}{\mathrm{argmin}}\, ||\boldsymbol{z} - \boldsymbol{x}|| \ . \end{gathered}$$

Here, $r > 0$ is a tuning variable for the numerical iteration, while $d\boldsymbol{u}$, dt, $d\boldsymbol{\Lambda}_N = \boldsymbol{\lambda}_N dt + \boldsymbol{P}_N d\eta$ and $d\boldsymbol{\Lambda}_T = \boldsymbol{\lambda}_T dt + \boldsymbol{P}_T d\eta$ are the differential measures with $\boldsymbol{P}_N d\eta$ and $\boldsymbol{P}_T d\eta$ representing the so-called atomic parts, i.e. the impulsive part of the impact and friction forces with $d\eta = \delta\left(t_i\right) dt$, where $\delta\left(t_i\right)$ is the Dirac delta function at t_i. Notice that (6) is now written as (measure) differential equations and (implicit) contact equations.

3 Gait Design

There are basically two ways to design a walking gait: (i) by deriving reference trajectories for each robot joint; (ii) by desiging control laws for the robot dynamics. In this section, we present two methods for the gait design that lead to different stable walking patterns.

3.1 Gait Design Preliminaries: Domains

A walking gait can be divided into several domains, as shown in Fig. 2. Each domain has own properties, needs own reference trajectories and control strategy.

1. *Push off*: At $t = t_1$, the robot is in double support. The goal is to lift the swing leg, by pushing off or by lifting the swing foot from the ground.
2. *Single support*: This domain starts at $t = t_2$ when all contact points on the swing foot become inactive. Often (not always), the goal is to reach knee lock of the swing leg by swinging the leg forward.
3. *Strike*: At $t = t_3$, the swing knee gets locked. The goal is to drive the swing foot to the ground.
4. *Double support*: At $t = t_4$, one of the contact points on the swing foot becomes active. At the same time, the swing leg and stance leg swap their functions. The goal is to interchange the weight support from one leg to another. This domain ends when the robot is ready to push off at $t = t_5$. After this, the gait moves to domain 1 again.

3.2 ZMP Based Gait Design

The method of ZMP is well-known and often used to design stable bipedal walking gaits. The ZMP is the location on the ground where the net moment generated from the ground reaction forces is strictly perpendicular to the ground [1]. As long as the ZMP lies inside the support polygon of the stand foot/feet, the biped does not tip over. When the ZMP lies on the edge of the support polygon, the robot might start tipping. Here, we present per domain shown in Fig. 2(a) how to design trajectories in each robot joint that satisfy the ZMP criterion for stable bipedal walking.

1. In this domain, the stance leg keeps the same configuration, $\boldsymbol{q}_{a1}(t) = \boldsymbol{q}_{a4}(t_1)$. This configuration is chosen such that ZMP remains above the stance foot during the complete swing phase. The swing foot needs to be lifted a distance h_{i1} from the ground. The initial and end positions of the swing ankle with respect to the hip are given by $\boldsymbol{p}_{i1}(t_1) := [x_{i1}, z_{i1}]$ and $\boldsymbol{p}_{i1}(t_2) := [x_{i1}, z_{i1} + h_{i1}]$, respectively. A Cartesian trajectory describing location of the swing ankle is then determined by fitting a sufficiently smooth function between $\boldsymbol{p}_{i1}(t_1)$ and $\boldsymbol{p}_{i1}(t_2)$. Trajectories with cosine velocity profiles and quintic polynomials [9] are standard options for such a fit. The swing leg joint trajectories $\boldsymbol{q}_{i1}(t)$ can now be calculated using the inverse kinematics.
2. For the same configuration in the stance leg as in the previous domain, which keeps ZMP above the stance foot, we have: $\boldsymbol{q}_{a2}(t) = \boldsymbol{q}_{a1}(t_2)$. The swing foot moves forward for a distance l_{i2} until the swing knee is locked. The initial and end positions of the swing ankle with respect to the hip are $\boldsymbol{p}_{i2}(t_2) := [x_{i2}, z_{i2}]$ and $\boldsymbol{p}_{i2}(t_3) := [x_{i2} + l_{i2}, z_{i2}]$, respectively. By fitting a sufficiently smooth Cartesian trajectory between $\boldsymbol{p}_{i2}(t_2)$ and $\boldsymbol{p}_{i2}(t_3)$, the swing leg joint trajectories $\boldsymbol{q}_{i2}(t)$ can be calculated using the inverse kinematics.
3. The stance leg keeps the same configuration in this domain, $\boldsymbol{q}_{a3}(t) = \boldsymbol{q}_{a2}(t_3)$, so ZMP remains above the stand foot. The swing moves downwards for a

distance $h_{i3} = -h_{i1}$. The initial position and end positions of the swing ankle with respect to the hip are $\boldsymbol{p}_{i3}(t_3) := [x_{i3}, z_{i3}]$ and $\boldsymbol{p}_{i3}(t_4) := [x_{i3}, z_{i3} - h_{i1}]$, respectively. Again, a Cartesian trajectory fit from $\boldsymbol{p}_{i3}(t_3)$ to $\boldsymbol{p}_{i3}(t_4)$ and inverse kinematics calculations lead to the swing leg joint trajectories $\boldsymbol{q}_{i3}(t)$.

4. Both feet of the robot are on the ground, which means a reduction of one dof. Here, we cannot treat the motions of two legs separately, since their motions are coupled. To resolve this situation, we divide the domain into two parts. In the first part we declare the stance leg as the master and the swing leg as the slave. This means that the stance leg determines the motion and that the swing leg has to follow. These motions are further constrained such as that ZMP remains above the support polygon, which is in this domain determined by both stand feet. We define the initial position of the hip with respect to the stance ankle: $\boldsymbol{p}_{a4}(t_4) := [x_{a4}, z_{a4}]$. The end position is defined as the position in which the robot stands straight up: $\boldsymbol{p}_{a4}\left(\frac{1}{2}(t_4 + t_5)\right) := [x_{a4} + l_{a4}, z_{a4} + h_{a4}]$. Since the legs are interconnected at the hip, the swing leg should perform a motion such that the position of the hip with respect to the swing ankle $\boldsymbol{p}_{i4}$ is the same as $\boldsymbol{p}_{a4}$ in Cartesian coordinates. Using simple goniometric relations, $\boldsymbol{p}_{i4}$ can be calculated from $\boldsymbol{p}_{a4}$. In the second part of this domain, the roles swap: the swing leg becomes the master and the stance leg the slave. We define the position of the hip with respect to the swing ankle: $\boldsymbol{p}_{i4}\left(\frac{1}{2}(t_4 + t_5)\right) := [x_{i4}, z_{i4}]$. The end position of this domain should be the initial one for domain 1: $\boldsymbol{p}_{i4}(t_5) := [x_{i4} + l_{i4}, z_{i4} + h_{i4}]$. Hence, the stance leg has to perform a motion which guarantees that $\boldsymbol{p}_{a4}$ is the same as $\boldsymbol{p}_{i4}$ in Cartesian coordinates. Again using simple goniometric relations, $\boldsymbol{p}_{a4}$ can be calculated from $\boldsymbol{p}_{i4}$. Using a cosine velocity profile to smoothly connect $\boldsymbol{p}_{i4}(t_4)$ and $\boldsymbol{p}_{i4}(t_5)$, as well as $\boldsymbol{p}_{a4}(t_4)$ and $\boldsymbol{p}_{a4}(t_5)$, we find a Cartesian trajectory for the position of the hip with respect to the swing and stance ankles, respectively. The swing and stance leg joint trajectories $\boldsymbol{q}_{i4}(t)$ and $\boldsymbol{q}_{a4}(t)$ can now be calculated using the inverse kinematics of the swing and stance legs, respectively.

3.3 LCW Gait Design

In the recent years limit-cycle walking (LCW) gaits [3] attract inrceasing attention. The underlying rationale is the use of the natural dynamics of the biped during walking, which yields certain benefits. First of all, the walking speed can significantly be increased in comparison with the ZMP based gaits. Secondly, the energy efficiency can be increased if the biped correctly makes use of gravity. Thirdly, the LCW gaits usually look much more human-like than ZMP-based. A LCW biped is not locally stable at every time instant, which is also the case with human walking. Unfortunately, the design of LCW gaits is seemingly far more complicated than the design of ZMP-based gaits. In this section we propose a general method to design a stable bipedal LCW gait. This gait design is not based on predefined joint trajectories, but is a result of feedback control applied on the bipedal robot. We first present four controllers that are used in the different domains of bipedal walk.

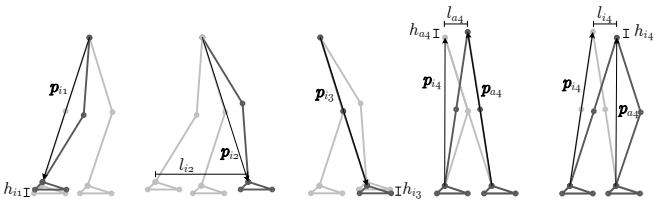

(a) ZMP based gait

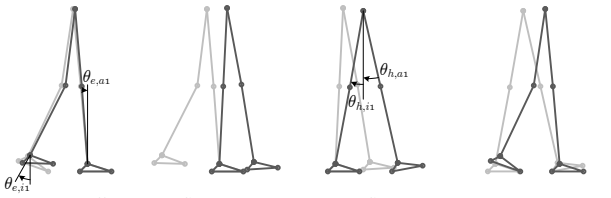

(b) LCW gait

Fig. 2. Snapshots of the two different gaits

– *Controlled symmetries*: To induce a passive behavior of the biped, this controller mimics the forces acting on the biped as if it would walk down a slope. The controller compensates for the actual gravitational forces, and at the same time it adds fictitious gravitational forces for the same robot configuration to mimic the dynamics of a passive dynamic walker of the same configuration as the considered bipedal robot [12], [13]:

$$\boldsymbol{\tau}_\beta = \boldsymbol{G}(\boldsymbol{q}) - \boldsymbol{G}(\boldsymbol{q} + \beta) \quad , \tag{7}$$

where $\boldsymbol{\tau}_\beta \in \mathbb{R}^{n_j}$ is the torque applied to the n_j actuated joints and β is the angle of the fictitious slope.

– *Foot Scuffing Prevention*: An additional foot scuffing prevention controller is used to prevent the swing foot from scuffing. This controller calculates a vertical force which exponentially grows when the swing ankle approaches the ground. This force is virtually applied to the swing ankle by mapping it to swing knee and hip torques. To prevent the swing leg from slowing down, at the same time a fraction of this force is, in the same manner, virtually applied in horizontal direction to the swing ankle.

$$\boldsymbol{\tau}_s = \boldsymbol{J}^T(\boldsymbol{q}_i) \begin{bmatrix} -\alpha_x e^{-\rho h_i(\boldsymbol{q}_i)} & -\alpha_z e^{-\rho h_i(\boldsymbol{q}_i)} \end{bmatrix}^T \quad , \tag{8}$$

where $\boldsymbol{\tau}_s \in \mathbb{R}^{n_i}$ is the torque applied to the n_i joints in the swing leg, $\boldsymbol{J}(\boldsymbol{q}_i)$ is the Jacobian of the swing leg to map the force to the joint torques, h_i is the height of the swing ankle, and α_x, α_z and ρ are tunable controller parameters.

– *Ankle Controller*: The ankle controller is a spring damper controller which adds some compliance to the ankle:

$$\tau_e = K_e^p \left(\theta_e^r - \theta_e\right) - K_e^d \dot{\theta}_e \ , \tag{9}$$

where θ_e^r is the reference angle, θ_e is the actual ankle angle, and K_e^p and K_e^d are tunable controller parameters.

– *Step Size Controller*: The step size controller regulates the angle between the swing and stance leg, and in that sense also regulates the size of a step. The controller is again a spring damper controller:

$$\tau_h = K_h^p \left(\theta_h^r - \theta_h\right) - K_h^d \dot{\theta}_h \ , \tag{10}$$

where θ_h^r is the reference angle, θ_h is the actual ankle angle, and K_h^p and K_h^d are tunable controller parameters.

In this work, the parameters of the given controllers are determined by trial and error. In the future, analytical computation of these parameters will be considered. Here, we explain how the controllers are used to achieve stable bipedal walk in different domains illustrated in Fig. 2(b).

1. In this domain, only the ankle controller is applied in the swing ankle with the reference angle $\theta_e^r = \theta_{e,i1}^r > 0$ to achieve push off, while in the stance ankle it is applied with $\theta_e^r = \theta_{e,a1}^r = 0$ to push the stance leg straight up.
2. The controlled symmetries controller is used in this domain to mimic the forces as if the robot was on a shallow slope. Additionally, the ankle controller is used in the swing ankle to keep the swing foot horizontally with respect to the ground; $\theta_e^r = \theta_{e,i2}^r(t)$, where $\theta_{e,i2}^r(t)$ is the angle between the current swing foot orientation and the ground. The ankle controller is also used in the stance ankle with $\theta_e^r = \theta_{e,a2}^r = 0$ to keep the stance leg straight up. Furthermore, the scuffing prevention controller is used on the swing ankle to prevent the swing foot from hitting the ground.
3. Here, the controlled symmetries controller is used again. Additionally, the step size controller is used in the stance hip with $\theta_h^r = \theta_{h,i3}^r > 0$ and in the swing hip with $\theta_h^r = \theta_{h,a3}^r = -\theta_{h,i3}^r$ to force the biped to make a certain step with predefined step size. Furthermore, the ankle controller is used to add some compliance in the swing and stance ankles, both with $\theta_{e,i3}^r = \theta_{e,a3}^r = 0$.
4. Here, the controlled symmetries controller and the ankle controller are used. The ankle controller works with $\theta_e^r = \theta_{e,i4}^r = \theta_{e,a4}^r = 0$ for both the swing and stance ankle.

4 Stability Analysis

Among the existing methods for stability analysis, the ZMP and the Poincaré return map methods are mostly used. In this section, we show conservatism of these methods by means of simulations. According to the definitions given in [6], a bipedal walking is stable if it is carried out without falling. A biped falls when any other point than points on the feet come in contact with the ground. Hence, we consider situations where the robot is allowed to touch the ground only with its feet. Sitting and crawling fall out of our scope.

4.1 ZMP Gait Analysis

We calculate the ZMP to qualify stability of a given gait. The ZMP can be determined by the moment balance around a point p on the foot with position $\boldsymbol{p}_p$ with respect to the base frame [1]:

$$\boldsymbol{M}_p = \dot{\boldsymbol{H}} - \boldsymbol{p}_c \times m_t \boldsymbol{g} + \left(\dot{\boldsymbol{P}} - m_t \boldsymbol{g}\right) \times \boldsymbol{p}_p \ , \tag{11}$$

where $\boldsymbol{M}_p = [M_x, M_y, M_z]^T$ is the moment acting in point p, $\dot{\boldsymbol{H}} = \left[\dot{H}_x, \dot{H}_y, \dot{H}_z\right]^T$ and $\dot{\boldsymbol{P}} = \left[\dot{P}_x, \dot{P}_y, \dot{P}_z\right]^T$ are the time derivatives of the angular and linear momenta of the biped with respect to the base frame, respectively, m_t is the total mass of the biped, $\boldsymbol{p}_c = [x_c, y_c, z_c]^T$ is the position of the center of mass, and $\boldsymbol{g}$ is the gravitational vector. By definition, the position of the ZMP, $\boldsymbol{p}_{ZMP} = [x_{ZMP}, y_{ZMP}, z_{ZMP}]^T$, is the point $\boldsymbol{p}_p$ for which $M_x = M_y = 0$. From this we can calculate the planar position of the ZMP with respect to the base frame:

$$x_{ZMP} = \frac{m_t g x_c - \dot{H}_y}{m_t g + \dot{P}_z} \ . \tag{12}$$

For small angular velocities, we use $\dot{H}_y = m_t \left(z_c \ddot{x}_c + x_c \ddot{z}_c\right)$ and $\dot{P}_z = m_t \ddot{z}_c$, in order to approximate (12) with the so called the cart-table model [14]:

$$x_{ZMP} = x_c - \frac{\ddot{x}_c}{g + \ddot{z}_c} z_c \ . \tag{13}$$

Now we can evaluate if the gaits illustrated in Figs. 2(a) and 2(b) are stable according to the ZMP criterion. For this, we simulate one step of the ZMP-based as well as the LCW gait. If the ZMP remains inside the support polygon, the ZMP criterion qualifies walking as stable. In Figs. 3(a) and 3(b), the ZMP trajectories for both gaits are plotted as functions of time, together with the support polygon limits. Please notice that for a planar biped, the support polygon is actually a line segment. These figures confirm what one would intuitively expect. The ZMP of the ZMP based gait stays inside the support polygon. According to the ZMP criterion this gait is stable. Nevertheless, the ZMP of the LCW gait does not stay inside the support polygon all the time. At time periods when the ZMP leaves the support polygion, the gait would be classified as unstable according to the ZMP stability criterion. This illustrative example let us realize that the ZMP stability criterion is too conservative to analyze the stability of an arbitrary gait. To the best of our knowledge, there is no similar illustration of conservatism of the ZMP criterion available in the literature.

4.2 Poincaré Return Map Gait Analysis

If a walking gait exhibits a cyclic pattern, then the biped realizing such a gait will return to the same state at the end of each cycle. One can consider a lower

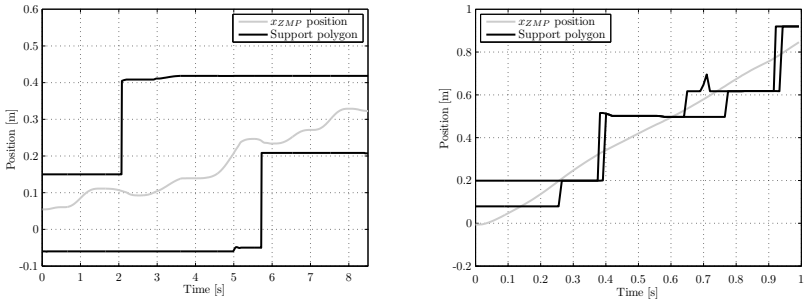

(a) ZMP based gait (b) LCW gait

Fig. 3. Position of the ZMP during one step

dimensional subspace $\boldsymbol{S}$ of the system state-space, the Poincaré return map, which is intersected by the cyclic motion. The intersection point is called a fixed point. For the stable periodic walking gait, the system state-trajectories return to approximately the same state after every step. One can make a Poincaré map at, for example, every start of a step, just after heel strike. According to the terminology of bipedal locomotion [2], [3], this mapping of the cyclic nonlinear dynamics is called the stride function. The stride function determines a transition between the current state and the state after one cycle:

$$\boldsymbol{q}_{k+1} = \boldsymbol{S}\left(\boldsymbol{q}_k\right) \quad . \tag{14}$$

Only if the motion is perfectly cyclic, then the state $\boldsymbol{q}$ is a fixed point $\boldsymbol{q}_f$:

$$\boldsymbol{q}_f = \boldsymbol{S}\left(\boldsymbol{q}_f\right) \quad . \tag{15}$$

The stability of the cyclic motion can be analyzed by perturbing the initial fixed point and checking if it returns to the fixed point after a finite number of cycles. Linearizing the stride function around these perturbations can tell us if the state will return to the fixed point:

$$\boldsymbol{S}\left(\boldsymbol{q}_f + \Delta\boldsymbol{q}\right) \approx \boldsymbol{q}_f + \boldsymbol{K}\Delta\boldsymbol{q} \ , \tag{16}$$

where $\boldsymbol{K} = \frac{\partial \boldsymbol{S}}{\partial \boldsymbol{q}}$ is the linear return matrix. This matrix determines if the state of the system returns to the fixed point for small perturbations. Namely, the motion is considered as stable if the eigenvalues of the matrix $\boldsymbol{K}$ fall inside the unit circle. If this is the case, then it is expected that the system state monotonously converges to the fixed point after each cycle. The smaller the absolute values of the eigenvalues, the faster the convergence to the limit cycle. Because of complexity of the biped dynamics, it is virtually impossible to find the stride function analytically. Therefore, the linear return matrix should be estimated by a finite difference approximation [2]. By doing so, we can analyze the gaits illustrated in Figs. 2(a) and 2(b) using the Poincaré return map stability

criterion. One step of each gait is simulated as many times as the number of states of the considered planar bipedal robot. At the beginning of every simulation, one state-coordinate is perturbed with respect to the initial state of the considered gait. From the results at the end of the step, we can calculate the linear return matrix and analyze the eigenvalues for each gait. The results that correspond to the two different gaits are presented in Table 1. The given results show that

Table 1. Eigenvalues of Poincaré return map

λ	ZMP	LCW
λ_1	0.3178	-0.4873
λ_2	$-0.0285 + 0.0730i$	$0.1326 + 0.0819i$
λ_3	$-0.0285 - 0.0730i$	$0.1326 - 0.0819i$
λ_4	$0.0545 + 0.0578i$	0.0222
λ_5	$0.0545 - 0.0578i$	-0.0159
λ_6	0.0127	0.0005
λ_7	$-3.1771e^{-4} + 4.2667e^{-4}i$	$1.5954e^{-5} + 4.5911e^{-5}i$
λ_8	$-3.1771e^{-4} - 4.2667e^{-4}i$	$1.5954e^{-5} - 4.5911e^{-5}i$
λ_9	$1.4851e^{-4}$	$-1.5233e^{-5}$
λ_{10}	$-2.7185e^{-5}$	$-1.9101e^{-5}$
λ_{11}	$1.2318e^{-5}$	$-3.1599e^{-6}$
λ_{12}	$-4.7939e^{-6}$	$8.8410e^{-7}$
λ_{13}	$-1.9989e^{-6}$	$-3.8626e^{-8}$
λ_{14}	$-3.3579e^{-7}$	$9.6776e^{-10}$

all eigenvalues of each gait lie within the unit disc. Consequently, the designed gaits are cyclically stable according to the Poincaré criterion. However, in the derivation of the stride function, we use a linearization of the system dynamics that are highly nonlinear and of a swtiching type. As shown in [8], the Poincare map for the swtiching type dynamics may experience further difficulties than we know from systems which are only nonlinear. A specific concern in this regard is whether the matrix $\boldsymbol{K}$ is well-defined. The Poincaré stability criterion can be applied to cyclic gaits only. The class of the periodic gaits is rather restrictive, which implies conservatism of the Poincaré stability method. In this aspect, the ZMP criterion is less conservative than the method of Poincaré, since periodicity of the gait is not a necessary condition for application of the ZMP criterion.

5 Conclusion

We model a bipedal robot as a system with unilateral constraints. This approach allows for the proper integration of ground contact and tangential friction force effects. In addition, a new methodology for the systematic design of limit-cycle walking (LCW) gaits is proposed. Finally, the planar biped model is used for simulation of two different walking gaits, based on the zero moment point (ZMP) and LCW principles, respectively. By means of simulations, we show serious

conservatism of the two mostly used criteria for stability analysis of bipedal walking: the ZMP criterion and the Poincaré return map method. Our results illustrate that fulfillment of the ZMP criterion is sufficient for stability, but this criterion is applicable to just a portion of complete state-space of the bipedal robot. Using the Poincaré return map method, we demonstrate that violation of the ZMP criterion does not necessarily mean that stable walking is not possible. Unfortunately, the Poincaré method can only be used to analyze the stability of periodic gaits only, which is a serious limitation. Periodicity of a gait is not necessary for application of the ZMP criterion. Consequently, neither criterion does offer a general stability qualification that includes all possible gaits an arbitrary biped can make. This raises a concern that the existing stability criteria are still in infancy regarding general qualification of stability of bipedal walking. Consequently, further research is needed to achieve a general stability criterion.

References

1. Vukobratovic, M., Borovac, B., Surla, D., Stokic, D.: Scientific Fundamentals of Robotics 7: Biped Locomotion. New York: Springer, the United States (1990)
2. Goswami, A., Espiau, B., Keramane, A.: Limit cycles in a passive compass gait biped and passivity-mimicking control laws. Autonomous Robots **4** (1997) 273–286
3. Hobbelen, D., Wisse, M.: Limit cycle walking. Humanoid Robots, Human-like Machines (2007)
4. Westervelt, E., Grizzle, J., Chevallereau, C., Choi, J., Morris, B.: Feedback control of dynamic bipedal robot locomotion. New York: CRC Press (2007)
5. Goswami, A.: Foot rotation indicator (FRI) point: A new gait planning tool to evaluate postural stability of biped robots. In: IEEE International Conference on Robotics and Automation, Citeseer (1999) 47–52
6. Pratt, J., Tedrake, R.: Velocity-based stability margins for fast bipedal walking. (First Ruperto Carola symposium: fast motions in biomechanics and robots)
7. Wight, D.L., Kubica, E.G., Wang, D.W.L.: Introduction of the foot placement estimator: A dynamic measure of balance for bipedal robotics. Journal of Computational and Nonlinear Dynamics **3** (2008) 1–9
8. Leine, R., Nijmeijer, H.: Dynamics and bifurcation of non smooth mechanical systems. Berlin: Springer Verlag, Germany (2004)
9. Spong, M., Hutchinson, S., Vidyasagar, M.: Robot modeling and control. New York: John Wiley and Sons, Inc. (2006)
10. Leine, R., van de Wouw, N.: Stability and convergence of mechanical systems with unilateral constraints. Berlin: Springer Verlag, Germany (2008)
11. Moreau, J.: Unilateral contact and dry friction in finite freedom dynamics. Nonsmooth mechanics and Applications (1988) 1–82
12. Spong, M., Bullo, F.: Controlled symmetries and passive walking. Automatic Control, IEEE Transactions on **50** (2005) 1025–1031
13. Sinnet, R., Ames, A.: 2d bipedal walking with knees and feet: a hybrid control approach. In: Decision and Control and 28th Chinese Control Conference, Joint 48th IEEE Conference on. (2009) 3200–3207
14. Siciliano, B., Khatib, O.: Springer handbook of robotics. Springer-Verlag New York Inc (2008)